Design of Microstrip Quadruplet Filters With Source–Load Coupling

Ching-Ku Liao and Chi-Yang Chang, *Member, IEEE*

***Abstract*—Quadruplet microstrip filters with source–load coupling are proposed to achieve similar skirt selectivity and/or in-band flat group delay as that of a sixth-order canonical form or an extracted pole microstrip filter. The diagnosis method of unwanted effects such as asynchronous resonant frequencies and unwanted couplings, which often occurs in the microstrip's open environment, is described in detail. A systematic design flow to implement a quadruplet microstrip source–load coupled filter with proper filter response is also provided. Two trial filters exhibited quasi-elliptical and flat group-delay response are designed and fabricated. Both theoretical and experimental results are presented.**

***Index Terms*—Diagnosis, flat group delay, microstrip quadruplet filter, source–load coupling.**

I. Introduction

HIGH-PERFORMANCE microstrip filters with high selectivity and linear in-band phase response has been studied over the last two decades [1]. Additional cross-coupling between nonadjacent resonators are often used to generate finite transmission zeros for high selectivity or linear phase. Naturally, the topology of the coupling network determines the number of finite transmission zeros, whereas the relative signs and magnitudes of the different coupling coefficients control the positions of finite transmission zeros. Some well-known topologies such as canonical form, cascade quadruplet (CQ), cascade trisection (CT) [1], and extracted-pole [2] have been successfully realized using a microstrip. For instance, Jokela [3] has shown that sixth-order canonical form filter can achieve both high selectivity and linear phase, which is attractive when comparing the passband insertion loss with the CQ filter. In the CQ configuration, a minimal of eighth order is required to generate the real-frequency transmission zeros pair for selectivity, and real axis transmission zeros pair for linear phase. An eighth-order CQ filter introduces more insertion loss than that of a sixth-order canonical form filter, but it gets the gain of independent transmission zeros where design and tuning becomes easy. However, there are some disadvantages attached to the canonical structure as mentioned in [2]. Besides, according to Jokela's paper [3], the in-band flat group delay and skirt selectivity can be obtained simultaneously, but a requirement of $M_{25} = 0$ should hold for easy implementation. This requirement simplifies the coupling routine, but greatly constrains the freedom of choice of filter response.

Manuscript received June 27, 2004; revised November 19, 2004. This work was supported in part by the National Science Council, R.O.C., under Grant NSC 93-2752-E-009-002-PAE.

The authors are with the Department of Communication Engineering, National Chiao Tung University, Hsinchu, Taiwan 30050, R.O.C. (e-mail: littleblue.ep86@nctu.edu.tw; mhchang@cc.nctu.edu.tw).

Digital Object Identifier 10.1109/TMTT.2005.850442

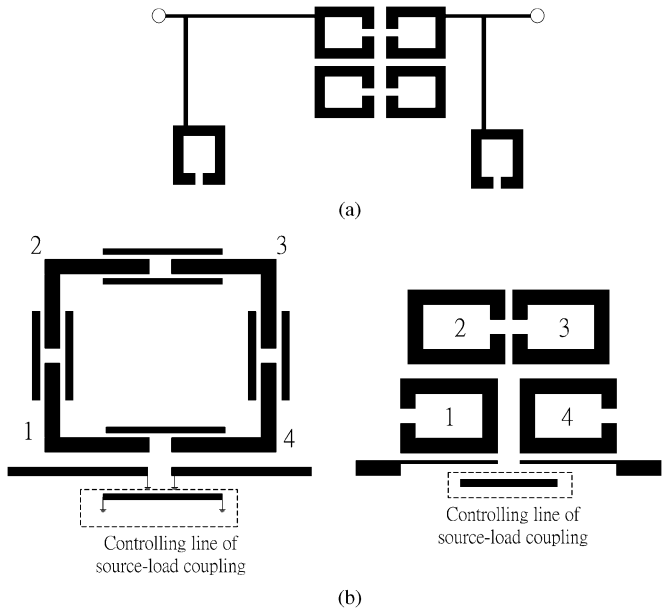

Fig. 1. Microstrip implementation for: (a) sixth-order quasi-elliptic filter with linear phase response using extracted-pole technique and (b) proposed quadruplet filter with source–load coupling.

To avoid the disadvantage of the canonical form filter, Yeo and Lancaster [2] proposed the extracted-pole microstrip filter, as shown in Fig. 1(a), where the concept is originally used in a waveguide filter. The extracted-pole filter depicts better control of finite transmission zeros than that of the canonical form filter, but it is relatively large due to the need of phase shifters. In this paper, we propose the fourth-order filter with source–load coupling, as shown in Fig. 1(b), to generate two pairs of transmission zeros as a sixth-order canonical form or eighth-order CQ filter does. The synthesis methods of the symmetric resonator filters with source–load coupling are well documented in the literature [4], [5]. A coupling diagram of the symmetric fourth-order filter with source–load coupling is shown in Fig. 2(a). However, in realistic implementation of a microstrip filter, the unwanted cross-couplings always exist and lead the coupling route to become complicated, as shown in Fig. 2(b). To identify all parameters corresponding to unwanted cross-couplings, frequency alignment, and source–load coupling, powerful computer-aided design (CAD) tools are needed. Recently, an elegant diagnosis method has been proposed to help the design of symmetric coupled-resonator filters [6]. However, the method in [6] has not taken the source–load coupling into account. In this paper, we propose a diagnosis scheme, which is applicable to arbitrary topologies with or without source–load coupling. This paper is organized as follows. In Section II, the phenomenon of asymmetric responses of a quadruplet filter is discussed

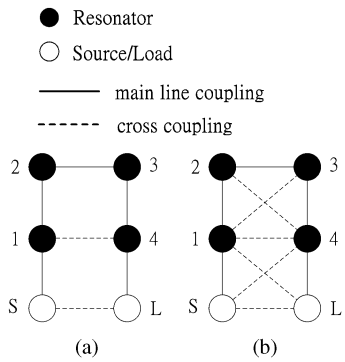

Fig. 2. Coupling and routing scheme of symmetric cross-coupled quadruplet filter with source–load coupling. (a) Ideal case. (b) Including the unwanted diagonal cross-couplings.

and design guidelines are provided. In Section III, the CAD method is introduced to extract the coupling matrix with prescribed topologies. In Section IV, the diagnosis method is applied to the design of the proposed filter. Both theoretical and experimental results are presented for comparison.

II. Asymmetric Frequency Response

The cross-coupled quadruplet filter is the well-known building block for generating a pair of finite transmission zeros, which can improve skirt selectivity or in-band group-delay flatness. The conventional coupling diagram of a quadruplet filter is similar to Fig. 2(a) , except that source–load coupling is excluded. The explicit relation between the finite transmission zeros and coupling coefficients can be expressed in the low-pass domain as follows [7]:

$$\Omega^2 = M_{23}^2 - \frac{M_{12}M_{23}M_{34}}{M_{14}}. \tag{1}$$

In (1), Ω is the normalized frequency and M_{ij} are the coupling coefficients in the low-pass prototype. The relation between Ω and actual frequency f is $\Omega = (f_0/\Delta f)(f/f_0 - f_0/f)$, where f_0 is the center frequency of the filter and Δf is the bandwidth of the filter. For improving the skirt selectivity of the filter, the finite transmission zeros are put in the real frequency axis and the relation $M_{12}M_{23}M_{34}M_{14} < 0$ must be satisfied. On the other hand, to generate the imaginary frequency transmission zeros for in-band group delay flatness, $M_{12}M_{23}M_{34}M_{14} > 0$ must hold. However, the unwanted diagonal cross-couplings occur easily in the microstrip cross-coupled filter due to the microstrip's open environment. Both unwanted diagonal cross-couplings and asynchronous resonant frequencies of resonators would destroy the ideal symmetric response of the reflection coefficient $|S_{11}|$ and transmission coefficient $|S_{21}|$. In [6] and [8], the authors have shown how to extract the unwanted diagonal cross-coupling and to adjust the resonant frequencies of resonators to compensate the distortion of return loss for a skirt selectivity filter. However, in the case of a flat group-delay filter, we find that the unwanted cross-couplings seriously degrade the flatness of in-band group delay and should be suppressed to a negligible level. Fig. 3 shows some examples to demonstrate the phenomena. In Fig. 3(a), an ideal response of the synchronous-tuned quadruplet filter with symmetric finite transmission zeros at $\Omega = \pm 2$ is shown. If the values of unwanted cross-couplings M_{13} and M_{24} are equal to -0.06, the frequency response after adjusting the resonant frequencies is shown in Fig. 3(b). It can be observed that the transmission zeros drift slightly and the height of $|S_{21}|$ bumps tilts. In many practical applications, this change of $|S_{21}|$ is acceptable. However, in the case of a flat group-delay filter, as shown in Fig. 3(c), the finite transmission zeros are located at $\Omega = \pm j1.55$. Setting $M_{13} = M_{24} = -0.06$, which is similar to the previous case, and adjusting the resonant frequency to optimize the in-band return loss, we would get the results shown in Fig. 3(d). It is obvious that the response of $|S_{21}|$ has negligible change, but the in-band group delay tilts seriously. In most linear phase filter applications, this tilting of group delay is not allowed.

From the above discussion, some observations are summarized as follows. First, higher order symmetric filters in folded form are hard to design since tuning of resonant frequencies is needed for compensating the in-band return-loss distortion. Besides, controlling more than one pair of finite transmission zeros and keep the return loss good is even more difficult. On the contrary, the source–load coupling has an extremely small contribution to the passband response and is much easier to implement an extra pair of transmission zeros. In other words, we can control the additional pair of finite transmission zeros and keep the original finite transmission zeros unchanged by merely adjusting source–load coupling without fine tuning another portion of the filter. Second, the unwanted cross-coupling is surprisingly harmful to the performance of the in-band flap group-delay response. The only way to implement a good in-band flap group-delay filter is to avoid the unwanted cross-coupling.

III. CAD Method for Filter Diagnosis

In Section II, we ignore the coupling term M_{L1}, M_{S4}, and M_{SL} to facilitate the discussion and give some design guidelines for the quadruplet filter. To get further insight about the correspondence between the proposed physical layout in Fig. 1(b) and the coupling diagram shown in Fig. 2(b), we introduce the CAD tool to extract the entire filter network parameters from the electromagnetic (EM) simulated results here.

The extraction method proposed here has two major steps. In the first step, we extract the $(N+2) \times (N+2)$ transversal coupling matrix, for the filter of order N from the EM simulated response as Garia-Lamperez *et al.* have done in [9]. In [9], the authors apply the Cauchy method to get the rational polynomial approximation of $S_{11}(\Omega)$ and $S_{21}(\Omega)$ from the EM simulated results, and then generate the corresponding transversal coupling matrix by the method proposed by Cameron [10]. Extracting the coefficients of the rational function by the Cauchy method is attractive since there is no need of calibrating the reference plane as that in [6] and [11]. In this step, we would get the transversal coupling matrix such as the following (take the proposed quadruplet filter for instance):

$$M = \begin{bmatrix} 0 & M_{S1} & M_{S2} & M_{S3} & M_{S4} & M_{SL} \\ M_{S1} & M_{11} & 0 & 0 & 0 & M_{1L} \\ M_{S2} & 0 & M_{22} & 0 & 0 & M_{2L} \\ M_{S3} & 0 & 0 & M_{33} & 0 & M_{3L} \\ M_{S4} & 0 & 0 & 0 & M_{44} & M_{4L} \\ M_{SL} & M_{1L} & M_{2L} & M_{3L} & M_{4L} & 0 \end{bmatrix}. \tag{2}$$

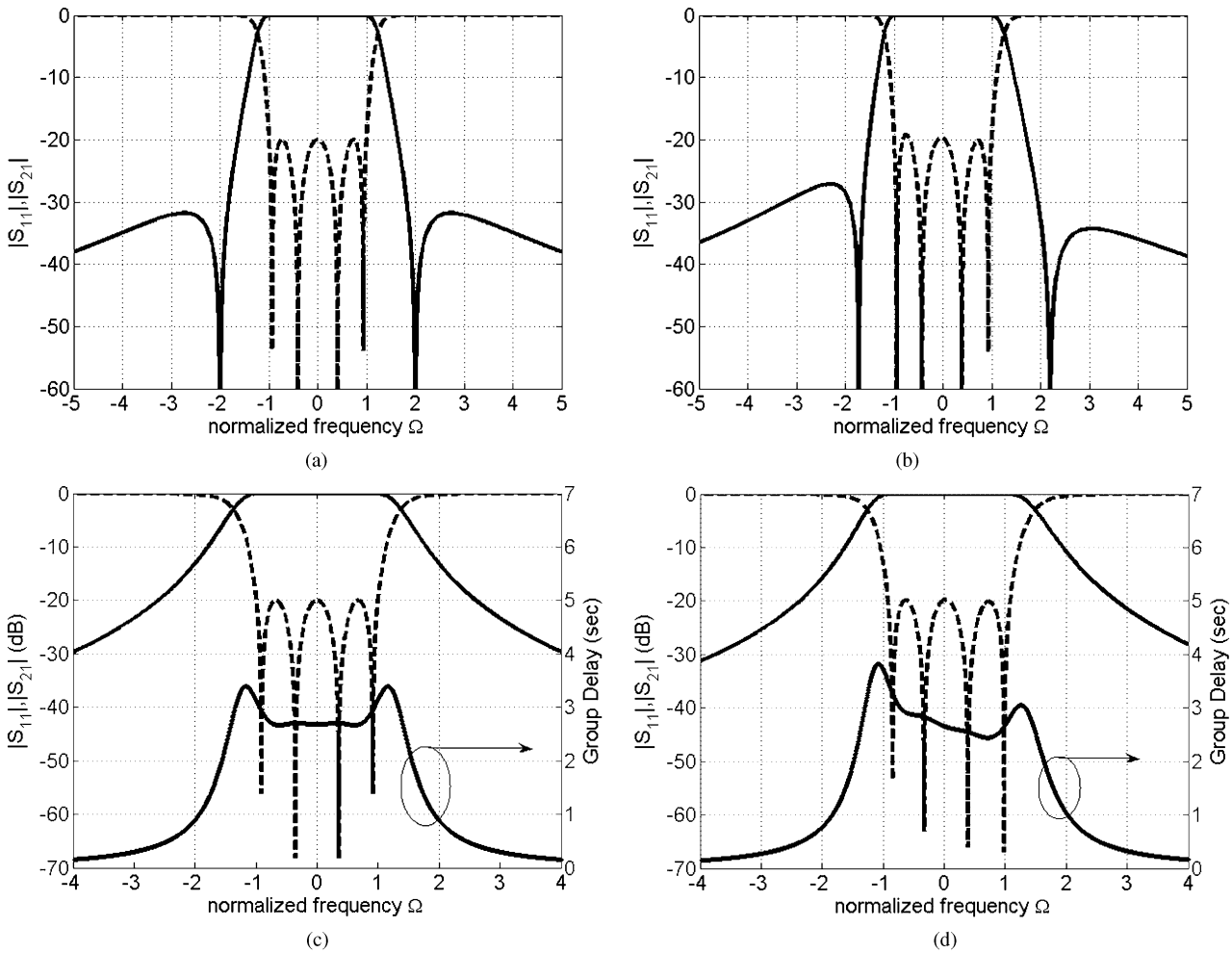

Fig. 3. Quadruplet filter with: (a) ideal quasi-elliptical response, (b) inclusion of unwanted cross-coupling, (c) ideal flap group-delay response, and (d) inclusion of unwanted cross-coupling.

The coupling matrix is related to the responses of $S_{11}(\Omega)$ and $S_{21}(\Omega)$ via the following equation [12]:

$$S_{11} = 1 + 2j[A^{-1}]_{11} \tag{3}$$

$$S_{21} = -2j[A^{-1}]_{N+2,1}. \tag{4}$$

Here, $A = \Omega[U_0] + [M] - j[R]$ and $\Omega = (f_0/\Delta f)(f/f_0 - f_0/f)$, $[U_0]$ is similar to the $(N+2)\times(N+2)$ identity matrix, except that $[U_0]_{11} = [U_0]_{N+2,N+2} = 0$, $[M]$ is the $(N+2)\times(N+2)$ symmetric coupling matrix, f_0 is the center frequency of the filter and Δf is its bandwidth, and $[R]$ is the diagonal matrix $[R] = \mathrm{diag}\{1, R_{\mathrm{loss}}, \ldots, R_{\mathrm{loss}}, 1\}$. R_{loss}, whose value is $(f_0/\Delta f)(1/Q_u)$, accounts for the resonator loss. Q_u is the unloaded quality factor of the resonator. Note that R_{loss} is set to be zero in the filter parameter-extraction process since the assumption of a lossless network must be satisfied in the extraction of $S_{11}(\Omega)$ and $S_{21}(\Omega)$ [9]. After getting the coupling matrix of prescribed topology, one can put R_{loss} back to calculate the practical filter response.

In the second step, the transversal coupling matrix is transformed into the prescribed topology. It is known that by applying the multiple similar transformations to the coupling matrix, one can get the equivalent coupling matrix with the same electrical performance as the original coupling matrix. Some methods may be found in the literature, which describe how to find the sequence of rotations (and the corresponding angles) required for obtaining a few specific topologies [10], [13], [14]. However, to the best of the authors' knowledge, how to transfer the transversal coupling matrix into the topology shown in Fig. 2 is still not known. Fortunately, one can apply the numerical optimization technique to determine the sequence and rotation angles of the multiple similar transformations as done by Macchiarella in [15]. The method reported in [15] works well for the synthesis of a filter with an order up to 12. The initial coupling matrix being used in [15] is the canonical folded or generic form, which corresponds to the filter of order N with a maximum of $N-2$ finite transmission zeros.

In this paper, we apply the optimization method as proposed by Macchiarella to transform the transversal coupling matrix to the prescribed topology, as shown in Fig. 2(b). Note that using the transversal coupling matrix as an initial coupling matrix extends the method of [15] applicable to a filter of order N with a maximum of N finite transmission zeros. In the following, we take the quadruplet filters as an example since they will be used in Section IV. Applying the multiple similar transformations to the transversal coupling matrix M in (2), we would get the new coupling matrix $\overline{M}$ and $\overline{M}$, which can be expressed as

$$\begin{aligned}\overline{M} &= (R_{23}\cdot R_{24}\cdot R_{25}\cdot R_{34}\cdot R_{35}\cdot R_{45}) \\ &\quad \cdot M \cdot \left(R_{45}^t \cdot R_{35}^t \cdot R_{34}^t \cdot R_{25}^t \cdot R_{24}^t \cdot R_{23}^t\right) \\ &= S(\vartheta_{23}, \vartheta_{24}, \ldots, \vartheta_{45}) \cdot M \cdot S^t(\vartheta_{23}, \vartheta_{24}, \ldots, \vartheta_{45})\end{aligned} \tag{5}$$

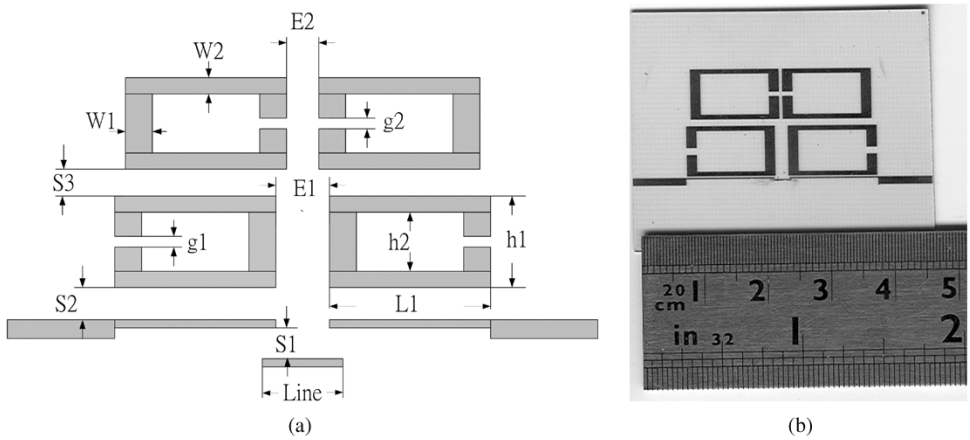

Fig. 4. (a) Quadruplet filter with the capacitive source–load coupling controlled by the controlling line. (b) Fabricated filter with dimension (in mils) $S1 = 4$, $S2 = 8$, $S3 = 41$, $E1 = 90$, $E2 = 20$, $W1 = 64$, $W2 = 30$, $h1 = 310$, $h2 = 250$, $g1 = 42$, $g2 = 26$, and Line $= 160$.

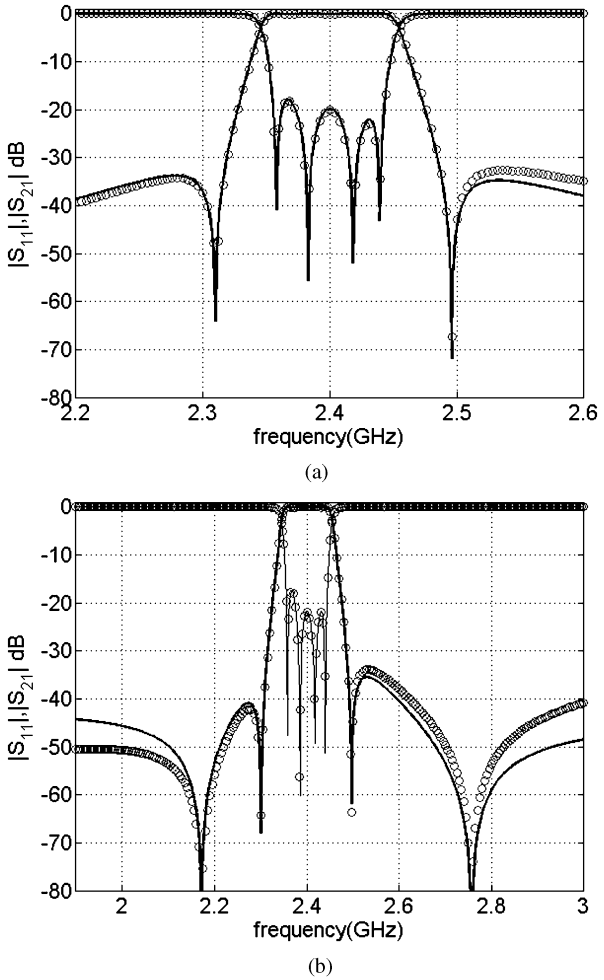

Fig. 5. (a) Response of quadruplet filter. (b) Response of quadruplet filter with controlling line of source–load coupling. Circle: EM simulated results. Solid line: circuit model.

where $R_{ij}(\vartheta_{ij})$ is the rotation matrix of order $N+2$ corresponding to pivot (i,j) and angle ϑ_{ij}. $R_{ij}(\vartheta_{ij})$ is defined as follows:

$$R_{ij}(i,i) = R_{ij}(j,j) = \cos(\vartheta_{ij})$$
$$R_{ij}(i,j) = -R_{ij}(j,i) = \sin(\vartheta_{ij})$$

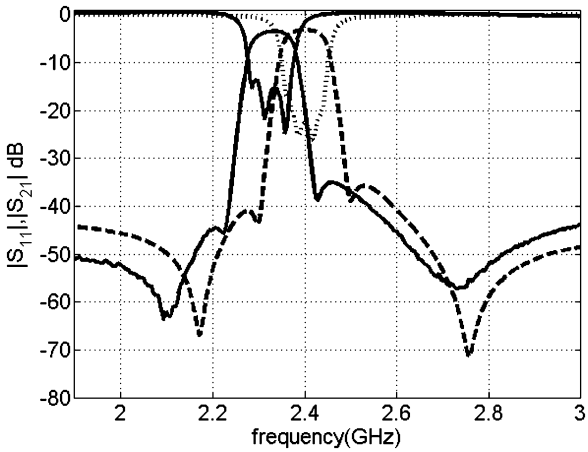

Fig. 6. Experimental and circuit model results. Solid line: experimental results. Dashed line: circuit model including loss term.

$$R_{ij}(k,k)|_{k\neq i,j} = 1, \qquad (i<j) \neq 1,\ N+2$$
$$R_{ij}(k,i)|_{k\neq i,j} = 0, \qquad R_{ij}(j,k)|_{k\neq i,j} = 0. \tag{6}$$

The cost function U for the topology shown is Fig. 2(b) is defined as

$$\begin{aligned} U(\vartheta_{23},\vartheta_{24},\ldots,\vartheta_{45}) &= |\overline{M}_{S2}|^2 + |\overline{M}_{S3}|^2 + |\overline{M}_{2L}|^2 + |\overline{M}_{3L}|^2 \\ &\quad + |\overline{M}_{11} - \overline{M}_{44}|^2 + |\overline{M}_{22} - \overline{M}_{33}|^2 \\ &\quad + |\overline{M}_{13} - \overline{M}_{24}|^2 + |\overline{M}_{S4} - \overline{M}_{1L}|^2. \end{aligned} \tag{7}$$

The first four terms in the cost function indicate which cross-coupling elements must vanish, while the last four terms indicate the symmetry of the coupling route. If the symmetric condition was not included in the cost function, we might get the nonphysical solutions. In the practical implementation of the minimization procedure, the Gauss–Newton method is used to determine the rotation angles $(\vartheta_{23},\vartheta_{24},\ldots,\vartheta_{45})$, which minimize the cost function U. Once the rotation angles are determined, we can get the corresponding coupling matrix $\overline{M}_{\mathrm{model}}$.

It should be mentioned that the proposed extraction scheme could be applied to arbitrary topologies once their feasibility has been assessed. Depending on the setting of different cost functions, different topologies can be obtained after multiple similar transformations. For the filter of order N, one can choose the

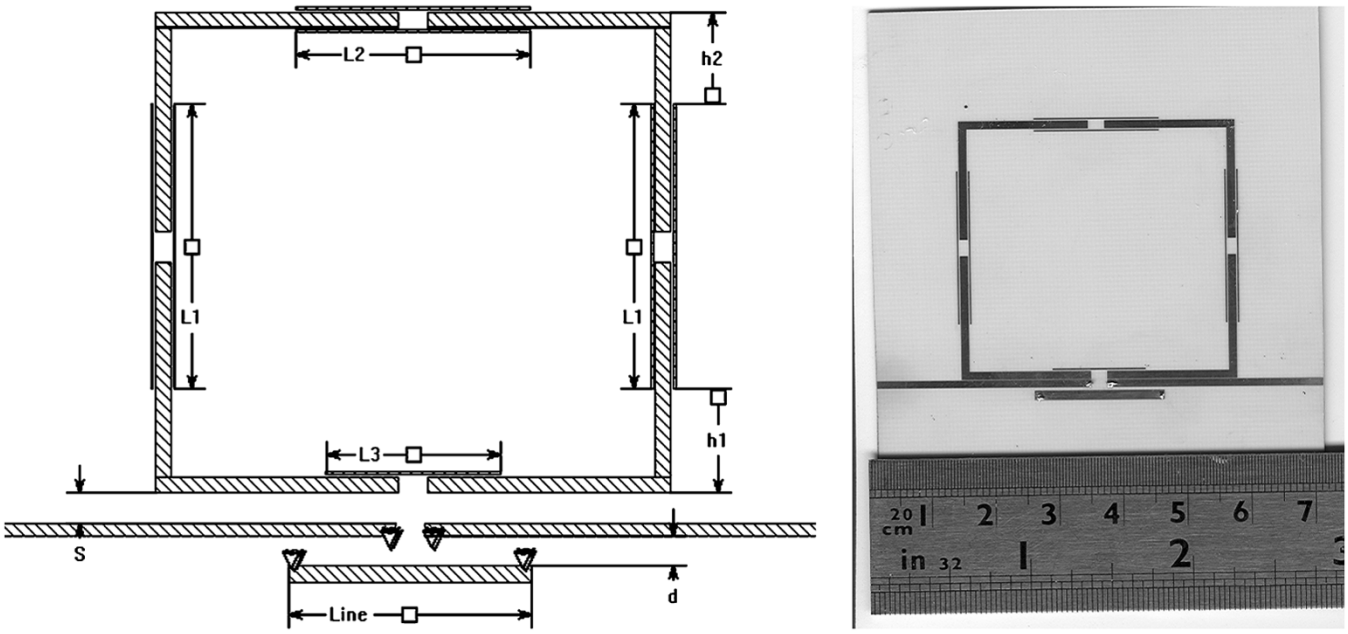

Fig. 7. (a) Quadruplet filter with the inductive source–load coupling controlled by the controlling line. (b) Fabricated filter with dimension (in mils) $d = 20$, Line $= 800$, $s = 4$, $L3 = 575$, $L1 = 940$, $L2 = 770$, $L3 = 575$, $h1 = 340$, and $h2 = 304$.

$N \times N$ coupling matrix or $(N+2) \times (N+2)$ coupling matrix as the initial coupling matrix, depending on the maximum number of finite transmission zeros. If the maximum number of finite transmission zeros is less than $N-2$, either an $N \times N$ [15] or $(N+2) \times (N+2)$ coupling matrix [16] can be chosen. Otherwise, the $(N+2) \times (N+2)$ transversal coupling matrix should be applied.

IV. Filter Design Examples

Here, we will focus on development of two novel quadruplet filters with source–load coupling and utilize the CAD tool introduced in Section III to do a diagnosis of the proposed filters. The design procedures are summarized as follows. Following the synthesis method described in [10], one would get the ideal coupling matrix with the topology shown in Fig. 2(a). The corresponding spacing between every resonator is determined through the characterization of the couplings, as described in [1, Ch. 8]. After EM simulation, the values of unwanted cross-couplings are extracted. Fixing the values of unwanted couplings, the optimization technique is then applied to determining the required frequency shifts of resonators and the change of other coupling elements to compensate the distortion of $|S_{11}|$ [17]. Two examples are given to show the design procedures. The first filter is designed to have two pairs of real frequency transmission zeros at normalized frequency $\Omega = \pm 2, \pm 6$ for skirt selectivity. The second filter is intended to have one pair of real frequency transmission zeros at normalized frequency $\Omega = \pm 4.5$ for selectivity and another pair at $\Omega = \pm j1.55$ for in-band flap group delay. The center frequency, fractional bandwidth, and maximum in-band return loss of both filters are 2.4 GHz, 3.75%, and 20 dB, respectively. The filters are built on a 20-mil-thick Rogers RO4003 substrate with $\varepsilon_r = 3.38$, $\tan\delta = 0.0021$. The commercial EM simulation software Sonnet 9.0 [18] is used to perform the simulation.

A. Quadruplet Filter With Two Pair of Real Frequency Transmission Zeros

The proposed layout is shown in Fig. 4. In order to see the effect of the controlling line, we exclude the controlling line at first and adjust the quadruplet filter following the previously mentioned procedures. After extracting the unwanted diagonal cross-couplings of the quadruplet filter and compensate them, we would get the EM simulated response, shown as circles in Fig. 5(a). Using the CAD tool developed in Section III together with the cost function defined in (7), the extracted coupling matrix M_1 (with the value of cost function $U = 10^{-7}$) is obtained as shown in the equation at the bottom of this page. The corresponding response of M_1 is also shown in Fig. 5(a), denoted as a solid line for comparison.

$$M_1 = \begin{bmatrix} 0 & 1.0089 & 0 & 0 & 0 & 0 \\ 1.0089 & -0.0021 & 0.8514 & -0.0090 & -0.1436 & 0 \\ 0 & 0.8514 & 0.0317 & 0.7380 & -0.0090 & 0 \\ 0 & -0.0090 & 0.7380 & 0.0317 & 0.8514 & 0 \\ 0 & -0.1436 & -0.0090 & 0.8514 & -0.0021 & 1.0089 \\ 0 & 0 & 0 & 0 & 1.0089 & 0 \end{bmatrix}$$

After adding the controlling line of source–load coupling, the EM simulated response is shown in Fig. 5(b), and is denoted as circles. The corresponding extracted coupling matrix M_2 (with the value of cost function $U = 10^{-7}$) is shown in the first equation at the bottom of this page. The corresponding response of coupling matrix M_2 is also shown in Fig. 5(b), denoted as a solid line.

Comparing M_1 and M_2, it can be easily observed that the introduction of the controlling line is only a small perturbation to the original quadruplet. In other words, the controlling line has a negligible contribution to the passband response. Besides, the existence of the tiny unwanted diagonal cross-couplings M_{S4} and M_{L1} in matrix M_2 explain why the response is asymmetric because the response becomes symmetric as M_{S4} and M_{L1} are excluded from M_2. Taking matrix M_2 into (3) and (4), and setting unloaded quality factor $Q_u = 150$, the results are shown in Fig. 6, denoted as dashed lines. The measured responses are also shown in Fig. 6, denoted as solid lines. Comparing the circuit model responses with measured responses, an excellent fit can be observed, except some frequency drift toward a lower frequency.

B. Quadruplet Filter for Flap Group Delay and Skirt Selectivity

As mentioned in Section II, the unwanted cross-couplings M_{13} and M_{24} would destroy the in-band group-delay flatness. To reduce the strength of unwanted couplings, we use the L-shaped resonator and arrange the resonators in square to maximize the distance between diagonal resonators, as shown in Fig. 7. The coupled lines with length L_1, L_2, and L_3 control the strength of coupling between L-shaped resonators, respectively. The inductive source–load coupling is effectively controlled by changing the length of the controlling line with both ends connected to the ground. Resonant frequencies of resonators can be tuned by adjusting the length $h1$ and $h2$. Following similar procedures in the previous design, we can get the extracted coupling matrix M_3, as shown in the second equation at the bottom of this page. The corresponding response of M_3 fits well with the EM simulated results, as shown in Fig. 8. Taking M_3 into (3) and (4) and setting unloaded quality factor $Q_u = 150$, we have the filter responses shown in Fig. 9 as doted lines. The experimental results are also shown in Fig. 9 as solid lines, which are similar to the circuit model results, except with a similar frequency drift as shown in the former example. The frequency drift might come from the discrepancy of the substrate dielectric constant. In other words, the dielectric constant ε_r might be greater than the data sheets' value of 3.38.

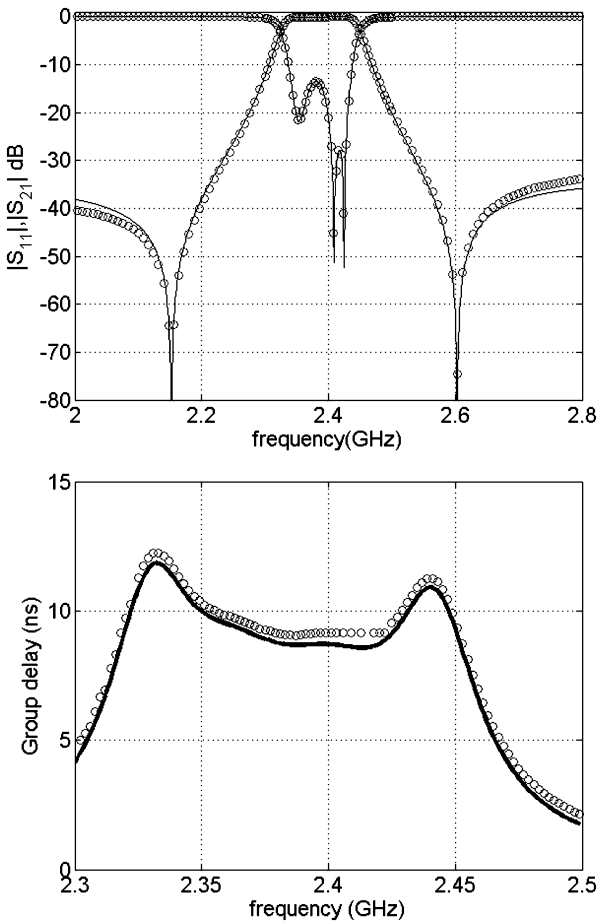

Fig. 8. Response of quadruplet filter with controlling line of source–load coupling. Circle: EM simulated results. Solid line: circuit model.

From the above two examples, we can conclude that the controlling line of source–load coupling can effectively adjusting the position of finite transmission zeros with negligible perturbation to the passband. It is suggested that one can design the symmetric folded coupled-resonator filter at first and then adds the controlling line to control the source–load coupling without fine-tuning the other portion of the filter. The design method may apply to a higher order symmetric folded coupled-resonator filter.

$$M_2 = \begin{bmatrix} 0 & 1.0189 & 0 & 0 & 0.0032 & 0.0035 \\ 1.0189 & -0.0120 & 0.8572 & -0.0057 & -0.1420 & 0.0033 \\ 0 & 0.8572 & 0.0204 & 0.7390 & -0.0058 & 0 \\ 0 & -0.0057 & 0.7390 & 0.0204 & 0.8571 & 0 \\ 0.0032 & -0.1420 & -0.0058 & 0.8571 & -0.0120 & 1.0189 \\ 0.0035 & 0.0033 & 0 & 0 & 1.0189 & 0 \end{bmatrix}$$

$$M_3 = \begin{bmatrix} 0 & -1.0945 & 0 & 0 & 0.0052 & 0.0099 \\ -1.0945 & 0.3663 & -1.0093 & -0.0274 & -0.1681 & 0.0054 \\ 0 & -1.0093 & 0.3402 & -0.6241 & -0.0272 & 0 \\ 0 & -0.0274 & -0.6241 & 0.3404 & -1.0089 & 0 \\ 0.0052 & -0.1681 & -0.0272 & -1.0089 & 0.3664 & -1.0936 \\ 0.0099 & 0.0054 & 0 & 0 & -1.0936 & 0 \end{bmatrix}$$

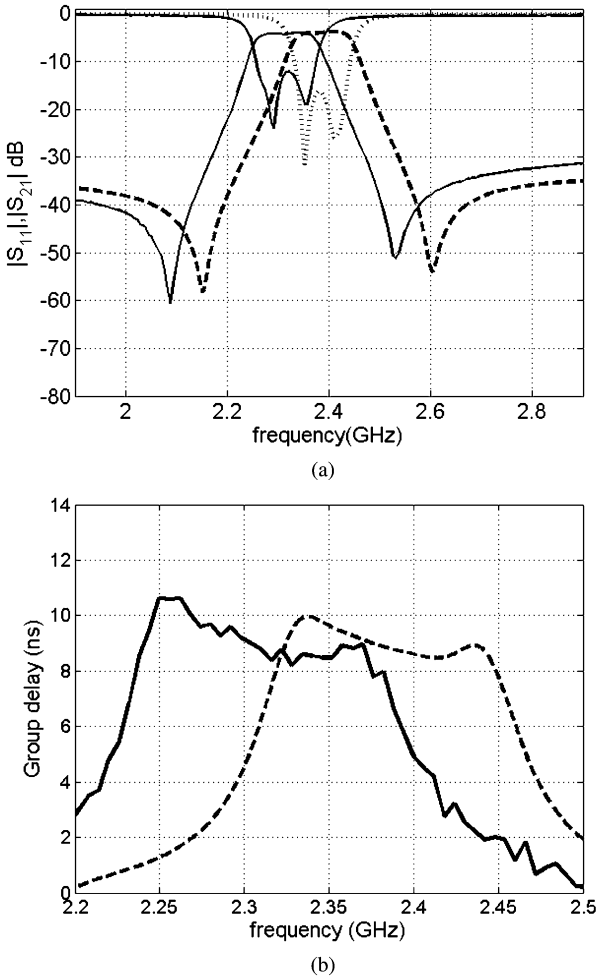

Fig. 9. Experimental and circuit model results. (a) Return loss and insertion loss. (b) Group delay. Solid line: experimental results. Dashed Line: circuit model including loss term.

V. Conclusion

In this paper, we have proposed some microstrip filter structures suitable to have source–load coupling to generate extra transmission zeros. The importance and difficulty of frequency alignment and avoiding the unwanted couplings in a microstrip filter have also been discussed. A novel diagnosis scheme has been proposed. Following a systematic design flow, two quadruplet filters with source–load coupling where one was designed for quasi-elliptical and another was designed for flat group-delay responses were fabricated, and the measured results agree well with that of theory. It has been shown that the diagnosis method described in this paper greatly helps to judge the unwanted effects in the microstrip quadruplet filter, where these effects were usually very difficult to specify in the microstrip's open environment.

References

[1] J. S. Hong and M. J. Lancaster, *Microstrip Filters for RF/Microwave Applications*. New York: Wiley, 2001.

[2] K. S. K. Yeo and M. J. Lancaster, "The design of microstrip six-pole quasi-elliptic filter with linear phase response using extracted-pole technique," *IEEE Trans. Microw. Theory Tech.*, vol. 49, no. 2, pp. 321–327, Feb. 2001.

[3] K. T. Jokela, "Narrow-band stripline or microstrip filters with transmission zeros at real and imaginary frequencies," *IEEE Trans. Microw. Theory Tech.*, vol. MTT-28, no. 6, pp. 542–547, Jun. 1980.

[4] J. R. Montejo-Garai, "Synthesis of N-even order symmetric filters with N transmission zeros by means of source–load cross coupling," *Electron. Lett.*, vol. 36, no. 3, pp. 232–233, Feb. 2000.

[5] S. Amari, "Direct synthesis of folded symmetric resonator filters with source–load coupling," *IEEE Microw. Wireless Compon. Lett.*, vol. 11, no. 6, pp. 264–266, Jun. 2001.

[6] H.-T. Hsu, Z. Zhang, K. A. Zaki, and A. E. Atia, "Parameter extraction for symmetric coupled-resonator filters," in *Proc. IEEE MTT-S Int. Microwave Symp.*, vol. 3, Jun. 2002, pp. 1445–1448.

[7] A. Atia and Williams, "New type of waveguide bandpass filters for satellite transponders," *COMSAT Tech. Rev.*, vol. 1, no. 1, pp. 21–43, 1971.

[8] S. Bila, D. Baillargeat, M. Aubourg, S. Verdeyme, P. Guillon, F. Seyfert, J. Grimm, L. Baratchart, C. Zanchi, and J. Sombrin, "Direct electromagnetic optimization of microwave filters," *IEEE Micro*, vol. 2, pp. 46–51, Mar. 2001.

[9] A. Garia-Lamperez, S. Llorente-Romano, M. Salazar-Palma, and T. K. Sarkar, "Efficient electromagnetic optimization of microwave filters and multiplexers using rational models," *IEEE Trans. Microw. Theory Tech.*, vol. 52, no. 2, pp. 508–521, Feb. 2004.

[10] R. J. Cameron, "Advanced coupling matrix synthesis techniques for microwave filters," *IEEE Trans. Microw. Theory Tech.*, vol. 51, no. 1, pp. 1–10, Jan. 2003.

[11] A. E. Atia and H.-W. Yao, "Tuning and measurements of couplings and resonant frequencies for cascaded resonators," in *Proc. IEEE MTT-S Int. Microwave Symp.*, vol. 3, Boston, MA, Jun. 2000, pp. 1637–1640.

[12] A. Garia-Lamperez, S. Llorente-Romano, M. Salazar-Palma, M. J. Padilla-Cruz, and I. H. Carpintero, "Synthesis of cross-coupled lossy resonator filters with multiple input/output couplings by gradient optimization," in *IEEE AP-S Int. Symp.*, vol. 2, Jun. 2003, pp. 52–55.

[13] H. C. Bell, Jr., "Canonical asymmetric coupled-resonator filters," *IEEE Trans. Microw. Theory Tech.*, vol. MTT-30, no. 9, pp. 1333–1340, Sep. 1982.

[14] R. J. Cameron, "General coupling matrix synthesis methods for Chebyshev filtering functions," *IEEE Trans. Microw. Theory Tech.*, vol. 47, no. 4, pp. 433–442, Apr. 1999.

[15] G. Macchiarella, "Accurate synthesis of inline prototype filters using cascaded triplet and quadruplet sections," *IEEE Trans. Microw. Theory Tech.*, vol. 50, no. 7, pp. 1779–1783, Jul. 2002.

[16] ——, "A powerful tool for the synthesis of prototype filter with arbitrary topology," in *Proc. IEEE MTT-S Int. Microwave Symp.*, Jun. 2003, pp. 1467–1470.

[17] H.-T. Hsu, Z. Zhang, K. A. Zaki, and A. E. Atia, "Parameter extraction for symmetric coupled-resonator filters," *IEEE Trans. Microw. Theory Tech.*, vol. 50, no. 12, pp. 2971–2978, Dec. 2002.

[18] *Em User's Manual*, Sonnet Software, Liverpool, NY, 2004.

Ching-Ku Liao was born in Taiwan, R.O.C., on October 16, 1978. He received the B.S. degree in electrophysics and M.S. degree in communication engineering from the National Chiao Tung University, Hsinchu, Taiwan, R.O.C., in 2001 and 2003, respectively, and is currently working toward the Ph.D. degree in communication engineering at the National Chiao-Tung University.

His research interests include the analysis and design of microwave and millimeter-wave circuits.

Chi-Yang Chang (S'88–M'95) was born in Taipei, Taiwan, R.O.C., on December 20, 1954. He received the B.S. degree in physics and M.S. degree in electrical engineering from National Taiwan University, Taiwan, R.O.C., in 1977 and 1982, respectively, and the Ph.D. degree in electrical engineering from The University of Texas at Austin, in 1990.

From 1979 to 1980, he was a Teaching Assistant with the Department of Physics, National Taiwan University. From 1982 to 1988, he was an Assistant Researcher with the Chung-Shan Institute of Science and Technology (CSIST), where he was in charge of the development of microwave integrated circuits (MICs), microwave subsystems, and millimeter-wave waveguide E-plane circuits. From 1990 to 1995, he returned to CSIST, as an Associate Researcher in charge of development of uniplanar circuits, ultra broad-band circuits, and millimeter-wave planar circuits. In 1995, he joined the faculty of the Department of Communication, National Chiao-Tung University, Hsinchu, Taiwan, R.O.C., as an Associate Professor and became a Professor in 2002. His research interests include microwave and millimeter-wave passive and active circuit design, planar miniaturized filter design, and monolithic-microwave integrated-circuit (MMIC) design.